Title
Self-Assembly of Two-Dimensional Perovskite Nanosheet Building Blocks into Ordered Ruddlesden–Popper Perovskite Phase

Journal
Journal of the American Chemical Society, 141(33)

ISSN
0002-7863

Authors
Liu, Yong
Siron, Martin
Lu, Dylan
et al.

Publication Date
2019-08-21

DOI
10.1021/jacs.9b06889

Peer reviewed

JACS
JOURNAL OF THE AMERICAN CHEMICAL SOCIETY
Communication
pubs.acs.org/JACS

Self-Assembly of Two-Dimensional Perovskite Nanosheet Building Blocks into Ordered Ruddlesden–Popper Perovskite Phase

Yong Liu,[†] Martin Siron,[‡] Dylan Lu,[†] Jingjing Yang,[†,§] Roberto dos Reis,[∥] Fan Cui,[†] Mengyu Gao,[‡] Minliang Lai,[†] Jia Lin,[†] Qiao Kong,[†] Teng Lei,[†] Joohoon Kang,[†,⊥,#,¶] Jianbo Jin,[†] Jim Ciston,[∥] and Peidong Yang*[,†,‡,§,¶]

[†]Department of Chemistry, University of California, Berkeley, Berkeley, California 94720, United States
[‡]Department of Materials Science and Engineering, University of California, Berkeley, Berkeley, California 94720, United States
[§]Materials Sciences Division, Lawrence Berkeley National Laboratory, Berkeley, California 94720, United States
[∥]National Center for Electron Microscopy, Molecular Foundry, Lawrence Berkeley National Laboratory, Berkeley, California 94720, United States
[⊥]Center for NanoMedicine, Institute for Basic Science (IBS), Seoul 03722, Korea
[#]Y-IBS Institute, Yonsei University, Seoul 03722, Korea
[¶]Kavli Energy NanoScience Institute, Berkeley, California 94720, United States

Supporting Information

ABSTRACT: The self-assembly of nanoparticles, a process whereby nanocrystal building blocks organize into even more ordered superstructures, is of great interest to nanoscience. Here we report the layer-by-layer assembly of 2D perovskite nanosheet building blocks. Structural analysis reveals that the assembled superlattice nanocrystals matche with the layered Ruddlesden–Popper perovskite phase. This assembly proves reversible, as these superlattice nanocrystals can be reversibly exfoliated back into their building blocks via sonication. This study demonstrates the opportunity to further understand and exploit thermodynamics to increase order in a system of nanoparticles and to study emergent optical properties of a superlattice from 2D, weakly attracted, perovskite building blocks.

Compared to bulk perovskites, quantum confined perovskites offer significant improvements, including stronger exciton binding energies, increased photoluminescence quantum yield, longer photon lifetime and increased stability.[1−8] Over the years, various groups have tuned the dimensionality, phase, and composition of perovskite nanocrystals. Typically, we can synthesize perovskites from 0D quantum dots,[9] 1D nanowires,[10,11] to 2D nanosheets.[6,12,13] We can tune the composition of ABX_3 perovskite by substituting various X-anions, A- and B-site cations.[14,15] We can also tune the arrangement of atoms in a perovskite crystal by tuning the phase,[16,17] due to the rich phase transitions available in the halide perovskite system. These are all ways to engineer and tune the optical properties at the atomic length scale. However, by systematically arranging the connection between the individual crystals themselves, we gain access to another level of tunability at a greater length scale. It is widely reported that superlattice nanocrystals offer emerging and interesting properties that are not found in their individual building blocks.[7,18,19] Typical strategies for creating such layered superlattices rely on complex methods, such as DNA grafting, direct layer-by-layer mechanical stacking, or liquid–air and liquid–liquid interface techniques.[20−25] A solvent-evaporation-based self-assembly process can produce high uniformity layered superlattices, but often yields an irreversible assembly.[26,27] In previous work, the intercalation of 2D sheets of metal-halide octahedral $[MX_6]^{4-}$ atomic building blocks with alkylammonium cations offered an approach to produce long-range ordered, well-crystalline 2D layered superlattices.[28] These layered structures typically formed Ruddlesden–Popper (RP) phase, an ideal class of perovskite analogues. RP crystals are of special interest due to their intrinsic confinement of the perovskite units and their increased stability.[29−31].

Currently, the most widely adopted method for the preparation of 2D layered perovskites involves a solution-processed crystallization.[32] This conventional crystallization technique often relies on either the slow cooling of concentrated solutions or quick solvent evaporation, which makes it difficult to engineer the shape, size, lattice structures and chemical compositions at the nanoscale level. Here, we address this challenge by synthesizing 2D perovskite nanosheets of precise thickness, which assemble, through a layer by layer process, into 2D layered RP phase superlattice nanocrystals with composition of $(C_8H_{17}NH_3)_2Cs_{n-1}Pb_nBr_{3n+1}$ (where n represents the number of $[PbBr_6]^{4-}$ octahedral layers). Figure 1A schematically illustrates the layer-by-layer self-assembly process, from individual perovskite nanosheets with an alkylammonium ligand surface to many superlattices matching the RP phase. The nanosheet building blocks were synthesized by a modified, ligand-assisted, air-free, hot-injection method[9] (Figures S1 and S2), which is similar to the synthesis reported by Manna et al.[12]

Received: June 28, 2019
Published: August 6, 2019

DOI: 10.1021/jacs.9b06889
J. Am. Chem. Soc. XXXX, XXX, XXX−XXX

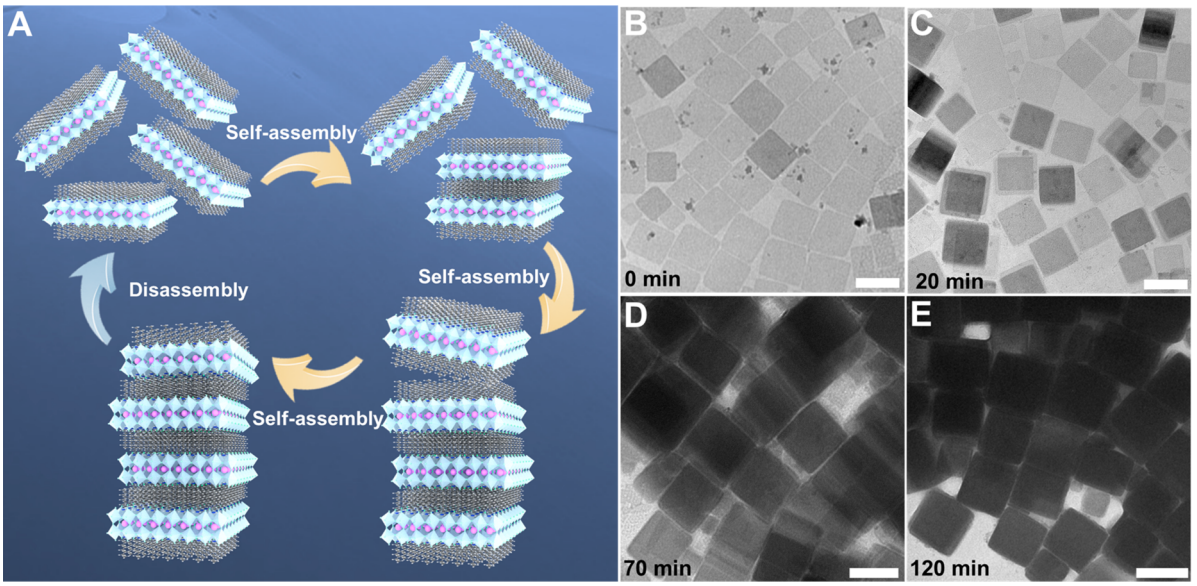

Figure 1. (A) Schematic illustration of the layer-by-layer, self-assembly of $C_8H_{17}NH_3$-capped $CsPb_2Br_7$ nanosheets into layered $(C_8H_{17}NH_3)_2CsPb_2Br_7$ superlattices. The superlattice nanocrystals can be reversibly exfoliated back into monolayer building blocks by sonication in toluene. (B) Initial $C_8H_{17}NH_3$-capped $CsPb_2Br_7$ nanosheets. (C, D) Superlattice intermediates. (E) Final $(C_8H_{17}NH_3)_2CsPb_2Br_7$ superlattice nanocrystals. Scale bar, 500 nm.

To analyze the self-assembly process, after synthesis, we took transmission electron microscopy (TEM) images at different stages of the process (Figure 1B−D and Figures S3−6). Initially, the $C_8H_{17}NH_3$-capped $CsPb_2Br_7$ building blocks were well dispersed in hexane, with limited assembled superlattices (Figure 1B and Figure S3). After 20 min, many of the crystals had increased contrast, indicating increased thickness of the superlattices (Figure 1C−D and Figures S4−7). Tapping-mode atomic force microscopy (AFM) images (Figure S8) taken after 30 min show that the thickness of these superlattices, taken as the assembly progressed, varied from three (about 6.3 nm), to eight (about 16.8 nm) and occasionally to tens of layers (25 layers, about 54.3 nm). As the self-assembly progressed, and the stacking of the building blocks continued, individual building blocks gradually decreased, forming many superlattices (Figure 1E). The overall thickness of the final nanocrystals superlattices were in the range of 100−400 nm after 4 h of self-assembly. Some TEM images taken during the assembly process reveal interlayer slipping between the periodic building blocks, which indicates the weakness of the force between the layers (Figure S9).

The square nanosheet building block has a lateral size of around ∼500 nm (Figure 2A). Energy-dispersive X-ray (EDX) analysis of single nanosheets (Figure S10A,B) shows an atomic ratio of Cs:Pb:Br of approximately 1:1.9:7.2. A high resolution TEM (HR-TEM) image of a single monolayer reveals a single-crystalline structure matching with an orthorhombic crystal phase (Figure 2B and Figure S11). The best matching from a series of simulated images is overlaid in Figure 2B, showing agreement with the experimental HR-TEM images. The average in-plane lattice constants of the monolayer were calculated to be $a \approx 8.2$ Å and $b \approx 8.4$ Å from selected-area electron diffraction (SAED) (Figure 2C). The well-dispersed monolayers in hexane exhibit a strong exciton absorption peak at 427 nm (inset of Figure 2D). Confocal photoluminescence (PL) of a single monolayer showed an emission peak centered at 431 nm (Figure 2D). The corresponding height profile obtained by tapping-mode AFM confirms the monolayers have a thickness around 2.2 nm (Figure 2E,F and Figure S10C,D).

After the self-assembly process is complete, uniform superlattice nanocrystals with an average lateral size of around 500 nm were formed (Figure 3A and Figure S12). After examining more than 10 individual assembled superlattices by EDX analysis (Figure S13 and Table S1), we found that the superlattices have an atomic ratio of Cs:Pb:Br of approximately 1:2:7. This ratio matches well with the 2D layered $(C_8H_{17}NH_3)_2CsPb_2Br_7$ RP phase crystal stoichiometry. The SAED images taken on a single nanocrystals superlattice (Figure 3B) confirm a crystalline structure with in-plane lattice constants of $a \approx 8.1$ Å and $b \approx 8.2$ Å, which are slightly smaller than those of the nanosheets measured by SAED. Powder X-ray diffraction (XRD) measurement of a drop-casted film of assembled crystals show characteristic periodic diffraction peaks of textured RP crystals: the (002), (004), (006) and (008) diffractions (Figure S14). Because of the nature of the textured sample, it is challenging to clarify the crystal structure of the superlattice. To further confirm the detailed crystal structure, we grounded the assembled crystals into a powder and loaded them on a glass substrate for grazing incidence wide angle X-ray scattering (GIWAXS) measurements (Figure S15). For comparison, we also synthesized the micron-sized $(C_8H_{17}NH_3)_2CsPb_2Br_7$ RP phase single crystals by solution-processed crystallization with the same organic ligands and inorganic perovskite precursors (Figures S16 and S17, crystal data summarized in Tables S2−4). Figure 3C shows that the in-plane diffraction peaks of the assembled superlattice nanocrystals match well with the crystal structure calculated from the $(C_8H_{17}NH_3)_2$ $CsPb_2Br_7$ RP phase micrometer-sized single crystals. The diffraction peaks from the powder XRD matches the *d*-spacing of the $(C_8H_{17}NH_3)_2CsPb_2Br_7$ RP nanocrystals captured with GIWAXS (Figure S15). Compared to the nanosheet's emission peak at 431 nm, the superlattice nanocrystals show a slightly red-shifted emission peak at 440 nm (Figure 3D). Our previous work demonstrated that such

DOI: 10.1021/jacs.9b06889
J. Am. Chem. Soc. XXXX, XXX, XXX−XXX

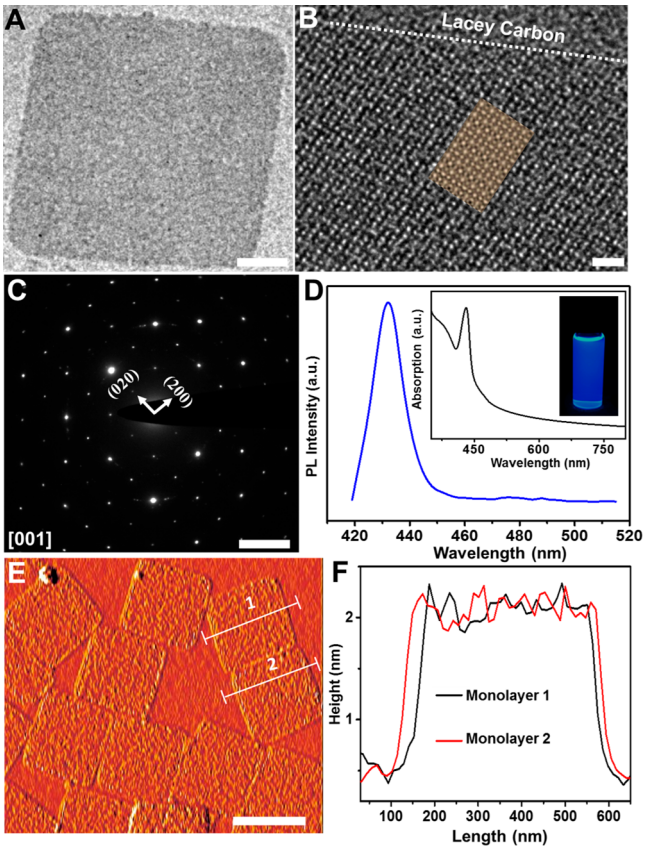

Figure 2. (A) TEM image of $C_8H_{17}NH_3$-capped $CsPb_2Br_7$ nanosheets. Scale bar, 100 nm. (B) HR-TEM image of a single $C_8H_{17}NH_3$-capped $CsPb_2Br_7$ nanosheet. Inset of panel B shows simulated TEM image. Scale bar, 1 nm. (C) SAED pattern taken from a single $C_8H_{17}NH_3$-capped $CsPb_2Br_7$ nanosheet. Scale bar, 5 nm^{-1}. (D) Confocal PL of a single $C_8H_{17}NH_3$-capped $CsPb_2Br_7$ nanosheet. Inset of panel D shows optical absorption of $C_8H_{17}NH_3$-capped $CsPb_2Br_7$ nanosheets dispersed in hexane solution. (E) AFM image. Scale bar, 500 nm. (F) Height profile of the $C_8H_{17}NH_3$-capped $CsPb_2Br_7$ nanosheets.

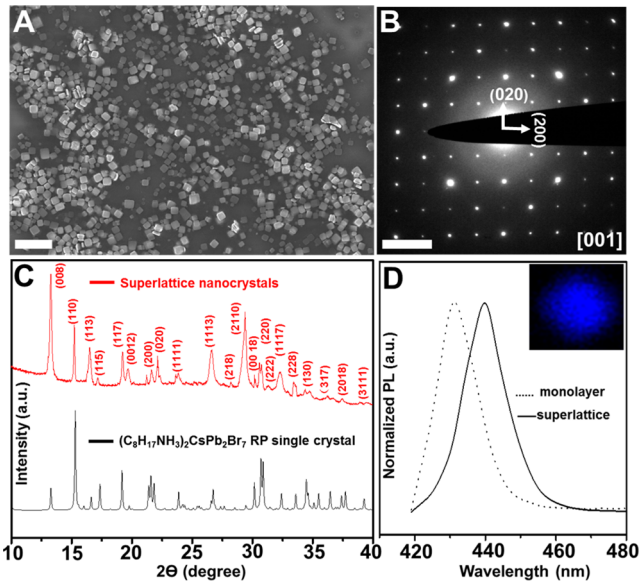

Figure 3. (A) SEM image of the 2D $(C_8H_{17}NH_3)_2CsPb_2Br_7$ superlattice nanocrystals, Scale bar, 2 μm. (B) SAED pattern taken from a single $(C_8H_{17}NH_3)_2CsPb_2Br_7$ nanocrystal. Scale bar, 2 nm^{-1}. (C) Comparison of wide-angle XRD pattern of $(C_8H_{17}NH_3)_2CsPb_2Br_7$ nanocrystals with $(C_8H_{17}NH_3)_2CsPb_2Br_7$ single crystals. (D) Confocal PL comparison of a single $(C_8H_{17}NH_3)_2CsPb_2Br_7$ superlattice nanocrystal and a single nanosheet building block. Inset shows confocal mapping of a single $(C_8H_{17}NH_3)_2CsPb_2Br_7$ superlattice nanocrystal.

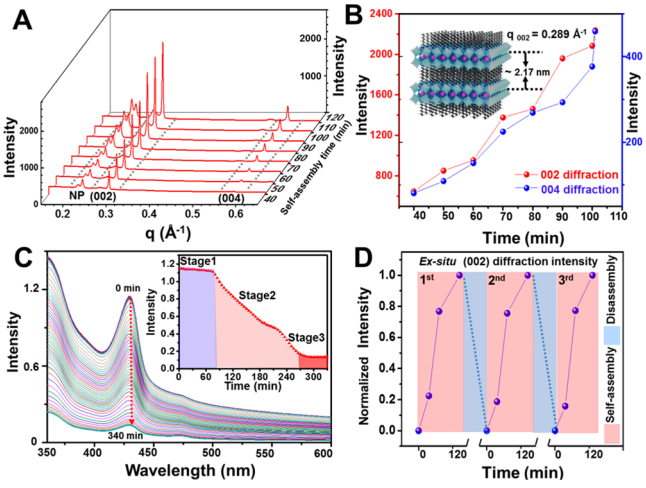

Figure 4. (A) *In situ* circularly averaged SAXS patterns taken at different self-assembly stages in hexane. (B) *In situ* SAXS diffraction peak intensity of the (002) and (004) reflection as a function of self-assembly time. (C) *In situ* UV−vis spectrum taken at different self-assembly stages in hexane. Inset shows evolution of the absorption peak intensity as a function of self-assembly time. (D) *Ex situ* XRD intensity of (002) diffraction peak as a function of self-assembly time during self-assembly and disassembly cycles.

slight PL red-shift could be induced by the lattice contraction upon assembly.[13]

Next, we used *in situ* synchrotron-based small-angle X-ray scattering (SAXS), in combination with *ex situ* small-angle XRD to monitor the self-assembly kinetics. Directly after synthesis, we loaded the fresh solution into a 2 mm capillary tube; we then took a SAXS scan periodically. At first, a weak scattering pattern was observed. As the reaction time progressed past 40 min, the weak diffraction peak at $q_{(002)}$ = 0.289 $Å^{-1}$ increased (Figure 4A). The $q_{(002)}$ matches with the (002) peak from the GIWAXS and powder XRD. The increased intensity of the (002) peak indicates that as the self-assembly progresses, the building blocks became more ordered and stacked face-to-face, along the [00l] crystallographic direction. After 90 min, higher order diffraction planes appeared (Figure 4A). From the (002) and (004) peaks, we can confirm the lamellar nature of the superlattices, with a lattice parameter of 2.2 nm, matching the thickness of the ligand covered building blocks. Figure 4B shows the peak intensity evolution of the (002) and (004) diffraction as a function of growth time. The strong periodicity along the [00l] direction from *in situ* SAXS and *ex situ* XRD indicates a highly ordered lamellar structure. Since we performed the *in situ* SAXS experiment directly after synthesis, there inevitably exists other nanoparticles (NP) in the solution. We attribute the *q*-vector at 0.228 $Å^{-1}$ to the assembly of these coexisting nanoparticles (Figure S18). These nanoparticles can generally be separated through centrifugation.

The *in situ* UV−vis spectrum complements the *in situ* SAXS and *ex situ* XRD data, showing similar kinetics (Figure 4C,D). Within the first 60 min, the absorption intensity at 427 nm did

DOI: 10.1021/jacs.9b06889
J. Am. Chem. Soc. XXXX, XXX, XXX−XXX

not change much. The lack of change in attenuation of the light indicates that the nanosheets stay at relatively similar concentration, while suspended in hexane. After 60 min, as shown in the inset of Figure 4C, the absorption intensity begins to decrease and the absorption position slightly red-shifts (from 427 to 429 nm) as a function of self-assembly time. The decrease in attenuation of the light indicates that the nanosheet concentration begins to decrease in solution. We can attribute this decrease in concentration to assembled crystals precipitating out of the solution. The settling down of these crystals is likely due to the increasing mass and decreasing surface area with ligand coverage as the assembly progresses. At the final stage, the weak absorption intensity at 429 nm remained unchanged for a continuous 4 h (inset of Figure 4C), indicating that the assembly has plateaued, and the process is in equilibrium.

A unique aspect of this colloidal system is the reversibility of the assembly, which has yet to be achieved with alkylammonium hybrid RP phase, or solvent-evaporation and Langmuir–Blodgett assembly techniques. The weak van der Waals forces between the building blocks allows for separation using mechanical force. By sonication in a weak polar solvent, the assembled superlattice can be disassembled back into its building blocks. We have tried several different solvents and found that sonication in toluene works the best. Under sonication, for around 15 to 25 min, the building blocks begin to detach from the assembled superlattice (Figure S19). We do note that at intense powers, sonication can break the monolayers due to the soft nature of the halide perovskite lattice. We can see signs of such structural damage in Figure S19E. Within 25 min, most superlattice are exfoliated back into their individual building blocks. The disassembled nanosheets were isolated from toluene by centrifugation, and then redispersed in hexane. Intriguingly, as shown in Figure 4D and Figure S20, these disassembled building blocks will reassemble back into a similar superlattice structure within 120 min, and such self/dis-assembly process can be well recycled for three times in the experiment.

The layer-by-layer self-assembly process exhibited in this system is a simple yet robust approach to generate large-scale 2D layered halide perovskite superlattices with atomic scale precision. Furthermore, the reversibility of this system gives us a way to systematically test properties that arise as a result of a more ordered system. This system may offer a general pathway for synthesizing other 2D layered superlattice nanomaterials for novel electronic and photonic applications.

■ ASSOCIATED CONTENT

Supporting Information

The Supporting Information is available free of charge on the ACS Publications website at DOI: 10.1021/jacs.9b06889.

Detailed experimental procedures, supporting results and additional figures (PDF)

■ AUTHOR INFORMATION

Corresponding Author

*p_yang@berkeley.edu

ORCID

Yong Liu: 0000-0002-1469-0757

Jingjing Yang: 0000-0002-1192-7368

Roberto dos Reis: 0000-0002-6011-6078

Teng Lei: 0000-0003-0356-1076

Joohoon Kang: 0000-0002-6578-2547

Peidong Yang: 0000-0003-4799-1684

Notes

The authors declare no competing financial interest.

■ ACKNOWLEDGMENTS

This work was supported by the U.S. Department of Energy, Office of Science, Office of Basic Energy Sciences, Materials Sciences and Engineering Division, under Contract No. DE-AC02-05-CH11231 within the Physical Chemistry of Inorganic Nanostructures Program (KC3103). GISAXS and GIWAXS measurements were carried out at beamline 7.3.3 at the Advanced Light Source, supported by the U.S. Department of Energy. TEM characterization work at the Molecular Foundry was supported by the Office of Science, Office of Basic Energy Sciences, of the U.S. Department of Energy under Contract No. DE-AC02-05CH11231. R. dR. and J.C. acknowledge support from the U.S. Department of Energy Early Career Research Program. Y.L. acknowledges the fellowship support from the Collaborative Innovation Center of Chemistry for Energy Materials (iChEM) and the International Postdoctoral Exchange Fellowship Program (No. 20160051). M.S. acknowledges fellowship support from the National Science Foundation Graduate Research Fellowship Program. J.K. also acknowledges IBS Global Postdoctoral Fellowship Award (IBS-R026-D1). We thank C. Zhu for the help with GIWAXS and fruitful discussions. We thank Y. Zhang and S. Wang for the AFM characterization.

■ REFERENCES

(1) Wang, N.; Cheng, L.; Ge, R.; Zhang, S.; Miao, Y.; Zou, W.; Yi, C.; Sun, Y.; Cao, Y.; Yang, R.; Wei, Y.; Guo, Q.; Ke, Y.; Yu, M.; Jin, Y.; Liu, Y.; Ding, Q.; Di, D.; Yang, L.; Xing, G.; Tian, H.; Jin, C.; Gao, F.; Friend, R. H.; Wang, J.; Huang, W. Perovskite light-emitting diodes based on solution-processed self-organized multiple quantum wells. *Nat. Photonics* **2016**, *10*, 699–704.

(2) Swarnkar, A.; Marshall, A. R.; Sanehira, E. M.; Chernomordik, B. D.; Moore, D. T.; Christians, J. A.; Chakrabarti, T.; Luther, J. M. Quantum dot-induced phase stabilization of alpha-$CsPbI_3$ perovskite for high-efficiency photovoltaics. *Science* **2016**, *354*, 92–95.

(3) Grancini, G.; Nazeeruddin, M. K. Dimensional tailoring of hybrid perovskites for photovoltaics. *Nature Rev. Mater.* **2019**, *4*, 4–22.

(4) Yang, S.; Niu, W. X.; Wang, A. L.; Fan, Z. X.; Chen, B.; Tan, C. L.; Lu, Q. P.; Zhang, H. Ultrathin two-dimensional organic-inorganic hybrid perovskite nanosheets with bright, tunable photoluminescence and high stability. *Angew. Chem., Int. Ed.* **2017**, *56*, 4252–4255.

(5) Akkerman, Q. A.; Rainò, G.; Kovalenko, M. V.; Manna, L. Genesis, challenges and opportunities for colloidal lead halide perovskite nanocrystals. *Nat. Mater.* **2018**, *17*, 394–405.

(6) Bekenstein, Y.; Koscher, B. A.; Eaton, S. W.; Yang, P.; Alivisatos, A. P. Highly luminescent colloidal nanoplates of perovskite cesium lead halide and their oriented assemblies. *J. Am. Chem. Soc.* **2015**, *137*, 16008–16011.

(7) Rainò, G.; Becker, M. A.; Bodnarchuk, M. I.; Mahrt, R. F.; Kovalenko, M. V.; Stöferle, T. Superfluorescence from lead halide perovskite quantum dot superlattices. *Nature* **2018**, *563*, 671–675.

(8) Imran, M.; Caligiuri, V.; Wang, M.; Goldoni, L.; Prato, M.; Krahne, R.; De Trizio, L.; Manna, L. Benzoyl halides as alternative precursors for the colloidal synthesis of lead-based halide perovskite nanocrystals. *J. Am. Chem. Soc.* **2018**, *140*, 2656–2664.

(9) Protesescu, L.; Yakunin, S.; Bodnarchuk, M. I.; Krieg, F.; Caputo, R.; Hendon, C. H.; Yang, R. X.; Walsh, A.; Kovalenko, M. V. Nanocrystals of cesium lead halide perovskites ($CsPbX_3$, X= Cl, Br,

DOI: 10.1021/jacs.9b06889
J. Am. Chem. Soc. XXXX, XXX, XXX–XXX

and I): novel optoelectronic materials showing bright emission with wide color gamut. *Nano Lett.* **2015**, *15*, 3692−3696.
(10) Zhang, D.; Eaton, S. W.; Yu, Y.; Dou, L.; Yang, P. Solution-phase synthesis of cesium lead halide perovskite nanowires. *J. Am. Chem. Soc.* **2015**, *137*, 9230−9233.
(11) Zhang, D.; Yu, Y.; Bekenstein, Y.; Wong, A. B.; Alivisatos, A. P.; Yang, P. Ultrathin colloidal cesium lead halide perovskite nanowires. *J. Am. Chem. Soc.* **2016**, *138*, 13155−13158.
(12) Shamsi, J.; Dang, Z.; Bianchini, P.; Canale, C.; Di Stasio, F.; Brescia, R.; Prato, M.; Manna, L. Colloidal synthesis of quantum confined single crystal $CsPbBr_3$ nanosheets with lateral size control up to the micrometer range. *J. Am. Chem. Soc.* **2016**, *138*, 7240−7243.
(13) Dou, L.; Wong, A. B.; Yu, Y.; Lai, M.; Kornienko, N.; Eaton, S. W.; Fu, A.; Bischak, C. G.; Ma, J.; Ding, T.; et al. Atomically thin two-dimensional organic-inorganic hybrid perovskites. *Science* **2015**, *349*, 1518−1521.
(14) Wong, A. B.; Lai, M.; Eaton, S. W.; Yu, Y.; Lin, E.; Dou, L.; Fu, A.; Yang, P. Growth and anion exchange conversion of $CH_3NH_3PbX_3$ nanorod arrays for light-emitting diodes. *Nano Lett.* **2015**, *15*, 5519−5524.
(15) Dou, L.; Lai, M.; Kley, C. S.; Yang, Y.; Bischak, C. G.; Zhang, D.; Eaton, S. W.; Ginsberg, N. S.; Yang, P. Spatially resolved multicolor $CsPbX_3$ nanowire heterojunctions via anion exchange. *Proc. Natl. Acad. Sci. U. S. A.* **2017**, *114*, 7216−7221.
(16) Kong, Q.; Lee, W.; Lai, M.; Bischak, C. G.; Gao, G.; Wong, A. B.; Lei, T.; Yu, Y.; Wang, L.-W.; Ginsberg, N. S.; Yang, P. Phase-transition-induced p−n junction in single halide perovskite nanowire. *Proc. Natl. Acad. Sci. U. S. A.* **2018**, *115*, 8889−8894.
(17) Lai, M.; Obliger, A.; Lu, D.; Kley, C. S.; Bischak, C. G.; Kong, Q.; Lei, T.; Dou, L.; Ginsberg, N. S.; Limmer, D. T.; Yang, P. Intrinsic anion diffusivity in lead halide perovskites is facilitated by a soft lattice. *Proc. Natl. Acad. Sci. U. S. A.* **2018**, *115*, 11929−11934.
(18) Nie, Z.; Petukhova, A.; Kumacheva, E. Properties and emerging applications of self-assembled structures made from inorganic nanoparticles. *Nat. Nanotechnol.* **2010**, *5*, 15−25.
(19) Nagaoka, Y.; Tan, R.; Li, R.; Zhu, H.; Eggert, D.; Wu, Y. A.; Liu, Y.; Wang, Z.; Chen, O. Superstructures generated from truncated tetrahedral quantum dots. *Nature* **2018**, *561*, 378−382.
(20) Dong, A.; Chen, J.; Vora, P. M.; Kikkawa, J. M.; Murray, C. B. Binary nanocrystal superlattice membranes self-assembled at the liquid−air interface. *Nature* **2010**, *466*, 474−477.
(21) Wang, C.; He, Q.; Halim, U.; Liu, Y.; Zhu, E.; Lin, Z.; Xiao, H.; Duan, X.; Feng, Z.; Cheng, R. Monolayer atomic crystal molecular superlattices. *Nature* **2018**, *555*, 231−236.
(22) Haigh, S.; Gholinia, A.; Jalil, R.; Romani, S.; Britnell, L.; Elias, D.; Novoselov, K.; Ponomarenko, L.; Geim, A.; Gorbachev, R. Cross-sectional imaging of individual layers and buried interfaces of graphene-based heterostructures and superlattices. *Nat. Mater.* **2012**, *11*, 764−767.
(23) Yu, W. J.; Li, Z.; Zhou, H.; Chen, Y.; Wang, Y.; Huang, Y.; Duan, X. Vertically stacked multi-heterostructures of layered materials for logic transistors and complementary inverters. *Nat. Mater.* **2013**, *12*, 246−252.
(24) Srivastava, S.; Nykypanchuk, D.; Fukuto, M.; Halverson, J. D.; Tkachenko, A. V.; Yager, K. G.; Gang, O. Two-Dimensional DNA-Programmable Assembly of Nanoparticles at Liquid Interfaces. *J. Am. Chem. Soc.* **2014**, *136*, 8323−8332.
(25) Lee, C.-H.; Lee, G.-H.; Van Der Zande, A. M.; Chen, W.; Li, Y.; Han, M.; Cui, X.; Arefe, G.; Nuckolls, C.; Heinz, T. F.; et al. Atomically thin p−n junctions with van der Waals heterointerfaces. *Nat. Nanotechnol.* **2014**, *9*, 676−681.
(26) Geuchies, J. J.; Van Overbeek, C.; Evers, W. H.; Goris, B.; De Backer, A.; Gantapara, A. P.; Rabouw, F. T.; Hilhorst, J.; Peters, J. L.; Konovalov, O.; et al. In situ study of the formation mechanism of two-dimensional superlattices from PbSe nanocrystals. *Nat. Mater.* **2016**, *15*, 1248−1254.
(27) Weidman, M. C.; Smilgies, D.-M.; Tisdale, W. A. Kinetics of the self-assembly of nanocrystal superlattices measured by real-time in situ X-ray scattering. *Nat. Mater.* **2016**, *15*, 775−781.
(28) Mitzi, D. B.; Feild, C.; Harrison, W.; Guloy, A. Conducting tin halides with a layered organic-based perovskite structure. *Nature* **1994**, *369*, 467−469.
(29) Tsai, H.; Nie, W.; Blancon, J.-C.; Stoumpos, C. C.; Asadpour, R.; Harutyunyan, B.; Neukirch, A. J.; Verduzco, R.; Crochet, J. J.; Tretiak, S.; et al. High-efficiency two-dimensional Ruddlesden−Popper perovskite solar cells. *Nature* **2016**, *536*, 312−316.
(30) Yuan, M.; Quan, L. N.; Comin, R.; Walters, G.; Sabatini, R.; Voznyy, O.; Hoogland, S.; Zhao, Y.; Beauregard, E. M.; Kanjanaboos, P.; et al. Perovskite energy funnels for efficient light-emitting diodes. *Nat. Nanotechnol.* **2016**, *11*, 872−877.
(31) Heinz, H.; Vaia, R.; Krishnamoorti, R.; Farmer, B. Self-assembly of alkylammonium chains on montmorillonite: effect of chain length, head group structure, and cation exchange capacity. *Chem. Mater.* **2007**, *19*, 59−68.
(32) Stoumpos, C. C.; Cao, D. H.; Clark, D. J.; Young, J.; Rondinelli, J. M.; Jang, J. I.; Hupp, J. T.; Kanatzidis, M. G. Ruddlesden-Popper Hybrid Lead Iodide Perovskite 2D Homologous Semiconductors. *Chem. Mater.* **2016**, *28*, 2852−2867.

DOI: 10.1021/jacs.9b06889
J. Am. Chem. Soc. XXXX, XXX, XXX−XXX